RAA 2014 Vol. **14** No. **8**, 1001–1010 doi: 10.1088/1674–4527/14/8/010
http://www.raa-journal.org *http://www.iop.org/journals/raa*

Research in Astronomy and Astrophysics

Identification of emission sources of umbral flashes using phase congruency *

Song Feng[1,2], Lan Yu[3], Yun-Fei Yang[1,2] and Kai-Fan Ji[1]

[1] Yunnan Key Laboratory of Computer Technology Application / Faculty of Information Engineering and Automation, Kunming University of Science and Technology, Kunming 650500, China; *ynkmfs@escience.cn*
[2] Key Laboratory of Solar Activity, National Astronomical Observatories, Chinese Academy of Sciences, Beijing 100012, China
[3] Department of Information Engineering, Yunnan Land and Resources Vocational College, Kunming 650217, China

Received 2013 November 20; accepted 2014 March 7

Abstract The emission sources of umbral flashes (UFs) are believed to be closely related to running umbral and penumbral waves, and are concluded to be associated with umbral dots in the solar photosphere. Accurate identification of emission sources of UFs is crucial for investigating these physical phenomena and their inherent relationships. A relatively novel model of shape perception, namely phase congruency (PC), uses phase information in the Fourier domain to identify the geometrical shape of the region of interest in different intensity levels, rather than intensity or gradient. Previous studies indicate that the model is suitable for identifying features with low contrast and low luminance. In the present paper, we applied the PC model to identify the emission sources of UFs and to locate their positions. For illustrating the high performance of our proposed method, two time sequences of Ca II H images derived from the *Hinode*/SOT on 2010 August 10 and 2013 August 20 were used. Furthermore, we also compared these results with the analysis results that are identified by the traditional/classical identification methods, including the gray-scale adjusted technique and the running difference technique. The result of our analysis demonstrates that our proposed method is more accurate and effective than the traditional identification methods when applied to identifying the emission sources of UFs and to locating their positions.

Key words: techniques: image processing — Sun: chromosphere — Sun: photosphere — sunspots — convection

1 INTRODUCTION

Umbral flashes (UFs) appear as transient brightenings observed in the Ca II H and K lines, and are found in almost every sunspot umbra. They represent one of the most exciting and enigmatic phenomena that are related to dynamic features of sunspots in the solar chromosphere, thus a great

* Supported by the National Natural Science Foundation of China.

number of observations have been used to reveal the nature of this attractive phenomenon. It is widely accepted that UFs, running penumbral waves and running umbral waves have the same emission sources, and they can be interpreted as different manifestations of the same oscillatory phenomenon in a sunspot (Beckers & Tallant 1969; Wittmann 1969; Moore 1973; Kneer et al. 1981; Spruit 1981; Rouppe van der Voort et al. 2003; Nagashima et al. 2007; Tziotziou et al. 2007; Socas-Navarro et al. 2009; Liang et al. 2011; Bharti et al. 2013). Many authors concluded that UFs are overstable oscillations from umbral dots in the solar photosphere. Beckers & Tallant (1969) considered that UFs and umbral dots in the solar photosphere are related, although they failed to find a one-to-one correspondence between them. Moore (1973) concluded that UFs and running penumbral waves have the same source which lies as low as the photosphere of the umbra. Utilizing the observations at La Palma with the Swedish Solar Telescope and the Dutch Open Telescope, Rouppe van der Voort et al. (2003) looked for the spatial coincidence between umbral dots and the emission sources of UFs. Using observations in the Ca II H line taken from the *Hinode*/SOT, Liang et al. (2011) found that each UF has an emission source and a relation with the running umbral waves.

Accurate identifications of the emission sources of UFs and their positions are a prerequisite for exploring their physical mechanism and the correlation between two types of running waves and umbral dots. A method based on using a gradient, like Sobel and Canny, can be used to identify the shape of UFs. The method has concentrated on the identification of local intensity discontinuities in an image, and it typically characterizes edge strength by the magnitude of the intensity gradient. Thus the perceived strength or significance of the edge is sensitive to variations in magnification. Another method based on intensity threshold, similar to a gradient based operator, also requires that the image features have distinct variations from the surroundings. This to say, image features with high contrast and luminance are a prerequisite when we use these two methods to identify the region of interest. However, it is extremely difficult to select an adaptive intensity threshold and/or gradient to objectively define the shape of UFs due to their low contrast and low luminance. Therefore, the technique of running difference is usually selected (Brisken & Zirin 1997; Rouppe van der Voort et al. 2003; Nagashima et al. 2007; Socas-Navarro et al. 2009; Liang et al. 2011, 2012) to highlight UFs. A running difference image is the difference between every image in the time sequence compared with the previous image. This method has two limitations:

(1) some quasi-static features, highlighting the continuous time-varying phenomena, are removed. However, they contain some important information, such as the position of the emission source generating UFs or running waves.
(2) The continuous time-varying features perhaps cannot be highlighted better due to a non-uniform intensity distribution in each image, even if the intensity of images in the time sequence is normalized. To sum up, it is timely to apply a novel image processing technique to accurately detect the emission sources of UFs and their positions.

An image feature could be better identified by its phase in the Fourier domain (Oppenheim & Lim 1981). The local phase of each frequency in the Fourier domain attains coherence at the point of the feature edge. Subsequently, a model of shape perception via phase congruency (PC) was proposed by Morrone et al. (1986) and Morrone & Owens (1987). Kovesi (1999, 2000) modified the model and demonstrated that the PC technique provides an invariant measure to determine a feature edge that is independent of luminance and contrast. Thus it can better solve the problem of the traditional methods which excessively depend on changes in image luminance and contrast. Therefore we used this technique to identify the emission sources of UFs and locate their positions.

The paper is structured as follows. The observations and data reductions are shown in Section 2. Section 3 introduces the basic concept of the PC technique. The comparison and evaluation of traditional analysis techniques of UFs are also detailed. Section 4 presents the results identified by our proposed method. Finally, the conclusions are given in Section 5.

2 OBSERVATIONS AND DATA REDUCTIONS

Our material consists of two sunspot image sequences taken from the Solar Optical Telescope (SOT) onboard *Hinode*. Both of them were obtained with the broadband filter imager (BFI: Tsuneta et al. 2008) of SOT, centered on the Ca II H (3968.5 Å) line. The pixel size of the images is 0.108″. For dark subtraction, flat-field correction and removing bad pixels, the standard reduction procedures provided by the SOT team were used. Then the images were carefully co-aligned by finding the displacement that gave the maximum cross-correlation between consecutive frames.

The first sequence was observed for a duration of 56 min (from 21:14 to 22:10 UT) on 2010 August 10, and the region was located at coordinates (156″, 46″) from the disk center. Because the original series contains some bad frames (i.e. frames with no data in all or part of the field of view), we only selected a smaller subset that had a duration of 40 min. The subset contains 113 continuum images with a cadence of ∼16 s. The field of view with 300×300 pixels used for our investigation is slightly smaller than the original one, but that contains the entire umbra.

As shown in Figure 1(a), the umbra was divided into two independent areas (Umbra A and Umbra B) by a light bridge. There is a UF in each area, and both of them are detailed in the following section. The other contains 215 images, and was observed for a duration of 1 h and 47 min (from 22:12–23:59 UT) with a cadence of ∼30 s on 2013 August 20. A field of view with 350×350 pixels was selected, and includes a fairly round sunspot. A sample of the sequence is shown in Figure 1(b).

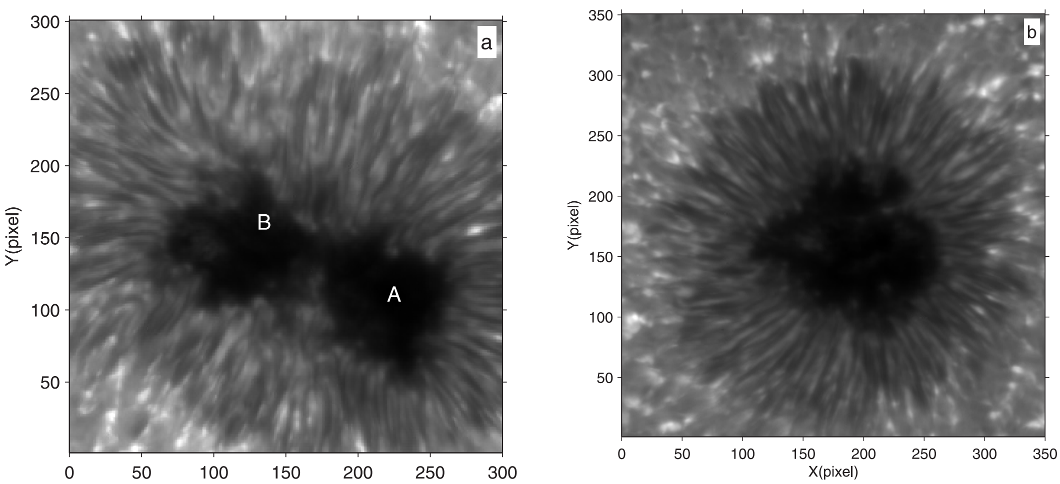

Fig. 1 (a) A snapshot of a Ca II H sample observed with the *Hinode*/SOT on 2010 August 10. There is a light bridge within the sunspot umbra, and the umbra is divided into two areas (Umbra A and Umbra B) by the light bridge. There is a UF in each area, and their evolutions are illustrated in Figs. 4 and 5, respectively. (b) A snapshot of a sample observed on 2013 August 20.

3 PHASE CONGRUENCY TECHNIQUE AND COMPARISON ANALYSIS

We first briefly describe the PC technique that is used to detect the emission sources of UFs, and then we compare our analysis results with traditional identification methods to evaluate the accuracy of our proposed method.

3.1 Phase Congruency

The spectral magnitude and phase in the Fourier representation play different roles when they are applied to describe the features in an image. Feature edges of an image can lead to phase coherence in Fourier components, whereas a corresponding statement cannot be made for spectral magnitude. Therefore, phase is more important than magnitude of the Fourier spectrum in feature recognition.

Morrone & Owens (1987) defined the phase congruency function in terms of the Fourier series expansion at a position x in a signal as

$$\mathrm{PC}(x) = \frac{\sum_n A_n \cos\left[\phi_n(x) - \bar{\phi}(x)\right]}{\sum_n A_n}, \quad (1)$$

where A_n represents the amplitude of the nth Fourier component and $\phi_n(x)$ represents the local phase of the nth Fourier component at the position x. $\sum_n A_n \cos[\phi_n(x) - \bar{\phi}(x)]$ denotes the local energy ($E(x)$) at the position x, seen in the schematic diagram of Figure 2.

Using Equation (1) to calculate a PC measure is rather awkward. Consequently, Kovesi (1999, 2000) developed a modified measure consisting of the cosine minus the magnitude of the sine of the phase deviation, and this produces a more localized response. This new measure also incorporates noise compensation

$$\mathrm{PC}^{\mathrm{1D}}(x) = \frac{\sum_n W(x)\lfloor A_n(x)\Delta\Phi_n(x) - T\rfloor}{\sum_n A_n(x) + \varepsilon}, \quad (2)$$

where $\Delta\Phi_n(x)$ is equal to $\cos[\phi_n(x)-\bar{\phi}(x)]-|\sin[\phi_n(x)-\bar{\phi}(x)]|$. T is the estimated noise influence (or the noise compensation), and ε is a small constant used to avoid division by zero. The term $W(x)$ is a factor that weights for frequency spread (congruency over many frequencies is more significant than congruency over a few frequencies). The symbols $\lfloor\rfloor$ denote that the enclosed quantity is equal to itself when its value is positive, and zero otherwise.

For a 2D signal of an image, the phase congruency function at a location (x, y) is specified by Equation (3)

$$\mathrm{PC}^{\mathrm{2D}}(x,y) = \frac{\sum_{\mathrm{o}}\sum_n W_{\mathrm{o}}(x,y)\lfloor A_{n\mathrm{o}}(x)\Delta\Phi_{n\mathrm{o}}(x,y) - T_{\mathrm{o}}\rfloor}{\sum_{\mathrm{o}}\sum_n A_n(x,y) + \varepsilon}, \quad (3)$$

where ‘o’ denotes the index over orientations and n is the scale of the wavelet applied to analyze an image.

The value of $\bar{\phi}(x)$ that maximizes the value of phase congruency is called local weighted mean phase angle (LWMPA) at one point in Equations (1), (2) and (3). The LWMPA is described as the angle corresponding to the orientation having the maximum local energy in Figure 2. It varies from a maximum of $\pi/2$, indicating a local intensity peak of a small region in an image, down to $-\pi/2$ indicating a local intensity trough. The case where LWMPA is equal to 0 means that the corresponding position is the boundary of the region of interest. For details of the PC measure and its implementation see Kovesi (1999, 2000).

3.2 Comparison Analysis

We carry out the LWMPA measure at each point based on the PC technique for identification of emission sources of UFs. We select 0 as a threshold in our method to extract the features of UFs within sunspot umbrae. Using the threshold for the LWMPA measure, a binary image is generated. The areas where the LWMPA measure is greater than the threshold can be regarded as some of the features of UFs. It is necessary to clearly mark the umbra-penumbra boundary for showing the behavior of UFs. Here we use the method developed by Zharkov et al. (2005) to identify the boundary. We first utilize a simultaneously observed G-band image of the first Ca II H image in

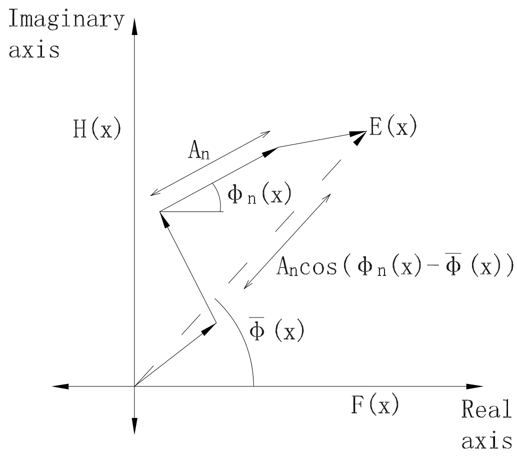

Fig. 2 Polar diagram showing the Fourier component at a location in the signal plotted head to tail. The plot illustrates the construction of the local energy ($E(x)$), sum of the Fourier amplitudes and phase congruency from the Fourier components of a signal. Adapted from Kovesi (1999).

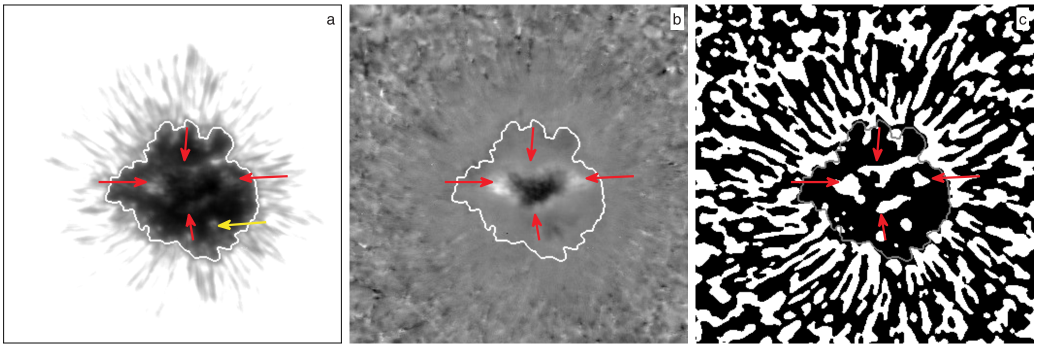

Fig. 3 (a) A gray-scale adjusted sample observed with the *Hinode*/SOT on 2013 August 20. The umbra-penumbra boundary is overlaid and denoted by a solid curve. The four red arrows indicate the bright patches (i.e., UFs). (b) The running difference image, which is the difference between the sample and the previous one in the time sequence. (c) The corresponding binary image generated by our proposed method. The bright areas within the sunspot umbra include UFs and PUDs.

the sequence to identify the boundary, and then overlay the boundary on each Ca II H image. The boundary is marked with a curve in the following figures.

To compare and validate the results identified by our method, we also use two traditional methods to identify UFs. First, the most straightforward way is to adjust the gray-scale of the original image. Secondly, the running difference image is selected to highlight UFs. Finally, we use the PC-based method to calculate the LWMPA measure of each point in the original image. The results treated by these three methods are shown in Figure 3(a), (b) and (c), respectively. We use a curve to mark the umbra-penumbra boundary in Figure 3. Figure 3(b) is the difference between the original image (i.e. Fig. 3(a)) and the previous image in the time sequence. Here, the bright patches represent the structures only appearing in the original image, while the dark patches describe the structures that only appear in the previous image. The binary image obtained from our method is shown in Figure 3(c). The bright patches within the sunspot umbra indicate the identified structures that include UFs and peripheral umbra dots (PUDs).

As shown in Figure 3(a), there are four bright patches identified by red arrows within the sunspot umbra, indicating UFs, but both their intensities and luminance are very low and their boundaries are blurry. There are several PUDs beside the marked bright patches within the sunspot umbra area. The PUDs are located at the inner umbra-penumbra boundary and are much brighter than the bright patches. One of the PUDs is marked with a yellow arrow in Figure 3(a). In Figure 3(b), the four red arrows indicate the positions of the bright patches that emerge in Figure 3(a). The two bright patches identified with left and right arrows are clear, but the others signified with upward and downward arrows can hardly be distinguished, although the two images are normalized with the same method before the running difference image is constructed. Thus, it is extremely difficult to obtain high precision for the bright patches and their corresponding boundaries using the two traditional methods. Fortunately, the bright patches are better identified and are located at their original positions in Figure 3(c), as well as the PUDs within the umbra. The bright patches quickly propagate towards the umbra-penumbra boundary in the evolution of UFs, but the intensity and position of PUDs are quasi-static. For this reason, the PUDs can hardly be located in Figure 3(b) because the running difference image can remove the quasi-static features. This demonstrates that the LWMPA measure based on the PC technique can efficiently detect the features with low luminance and low contrast. It is a prerequisite to identify and locate the emission sources of UFs. The term "bright patches" only denotes the UFs, and excludes the PUDs in the following section.

4 RESULTS

Based on the result of each image in the two sequences, we created two movies for accurately investigating the emission sources of UFs. The movies can be found at the site: *http://www.raa-journal.org/files/* .

The movies vividly demonstrate the phenomena: (i) UFs appear periodically within each sunspot umbra area; (ii) bright patches are generated by an emission source, and then quickly propagate towards the umbra-penumbra boundary around their corresponding source. The cases are detailed in Figures 4, 5 and 6.

The first case shown in Figure 4 is located in Umbra A of the first sequence, and the sequence that is a cutout from frames 82 to 89. The first row is the original sequence of images. The second row is the corresponding gray-scale adjusted images. The running difference images are shown in the third row. Our results are shown in the bottom row. Except for the sunspot umbral area, we remove the others in order to highlight the evolution of UFs. The emission source position of the UF is marked with a red rectangle in each frame.

As shown Figure 4, we find that a bright patch first appears at the position marked with a red rectangle in frame 83, rather than in frame 82, indicating that a UF is generated there. However, it is difficult to find the corresponding phenomenon in the running difference images. It is also hard to search for the corresponding phenomenon in the gray-scale adjusted images. The brightening phenomenon is validated by the running difference images and gray-scale adjusted ones in frames 85 and 86. However, the area of the bright patch has been increased and the patch starts moving toward the umbra-penumbra boundary in frames 85 and 86. The brightness of the UF continually increases, and its shape continues to expand in frame 87. Several irregular bright patches begin to form and simultaneously propagate towards the umbra-penumbra boundary in frames 88 and 89.

A bright patch periodically appears at the emission source position within the sunspot umbra in the following frames of the movies, and then propagates outward when forming a large patch around the dot-like source. Sometimes the patch can split multiple bright patches and simultaneously propagate outward.

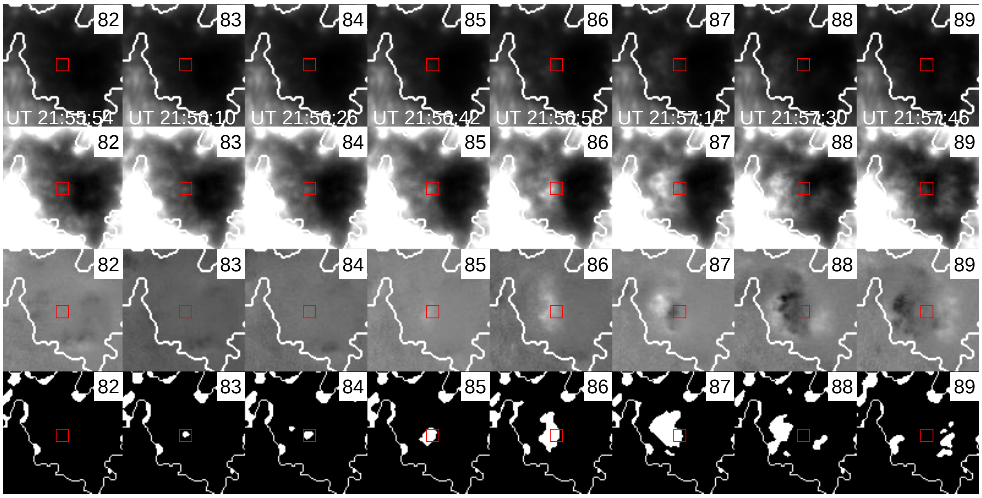

Fig. 4 An illustration of the UF that is located in Umbra A of the first sequence. *The first row panel*: a sequence that is a cutout from the original Ca II H images. *The second row panel*: a sequence that is a cutout from the gray-scale adjusted images. *The third row panel*: a sequence that is a cutout from the running difference images. *The fourth row panel*: the results identified by our proposed method. The bright patches near the umbra-penumbra boundary are some PUDs. The emission source position of the UF is marked with a red rectangle. The bright patches are generated by the emission source position, and then quickly propagate outward.

Another case shown in Figure 5 is located in Umbra B of the first sequence, and it is a sequence that is a cutout is from frames 39 to 46. Similar to the event shown in Figure 4, the emission source position of the UF is marked with a red rectangle in each frame. A bright patch first appears at the emission source position of frame 39. However, the phenomenon fails to be found in the corresponding running difference image. Then its shape continuously expands and the intensity continuously increases from frames 40 to 42. The intensity of the source position peaks at frame 42. Subsequently (from frames 43 to 45) the bright patch becomes more diffused due to its irregular shape, and disappears at the boundary of the umbra-penumbra in frame 46.

Similar to the above two cases (Figs. 4 and 5), Figure 6 also illustrates a UF and its emission source in the second sequence. We select the sequence that is a cutout from frames 15 to 20. Similarly, the emission source position of the UF is marked with a red rectangle in each frame. As shown in frame 16, a bright patch first appears at the emission source position. Its shape continuously expands, and splits into several bright patches in frame 17. Subsequently, (from frame 18 to 20) the bright patches become more irregular, and quickly propagate towards the umbra-penumbra boundary.

From the above three cases, we can see that each UF has an emission source. Moreover, compared to the traditional methods, the emergence of UFs can be more accurately identified with our approach. Meanwhile, it can find the phenomenon earlier than the traditional methods.

Figures 4 and 5 validate the high performance. As shown in Figure 6, the emission source position of the UF is detected simultaneously using both the running difference image and our proposed method, implying that the time cadence of 30 s in the second sequence does not suffice for accurately identifying the emission source of UFs and for locating their position.

Using the results shown in Figures 4 and 5, we obtain the intensity of the emission sources of the UFs, and calculate the ratio of their mean intensity to the median value of the corresponding region

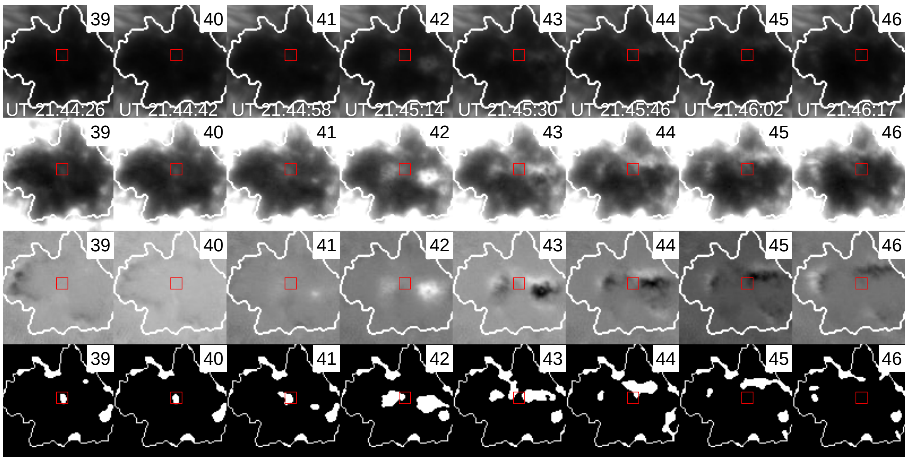

Fig. 5 An illustration of another UF. It is located in Umbra B of the first sequence. Similarly, the emission source position is also marked with a red rectangle in each frame.

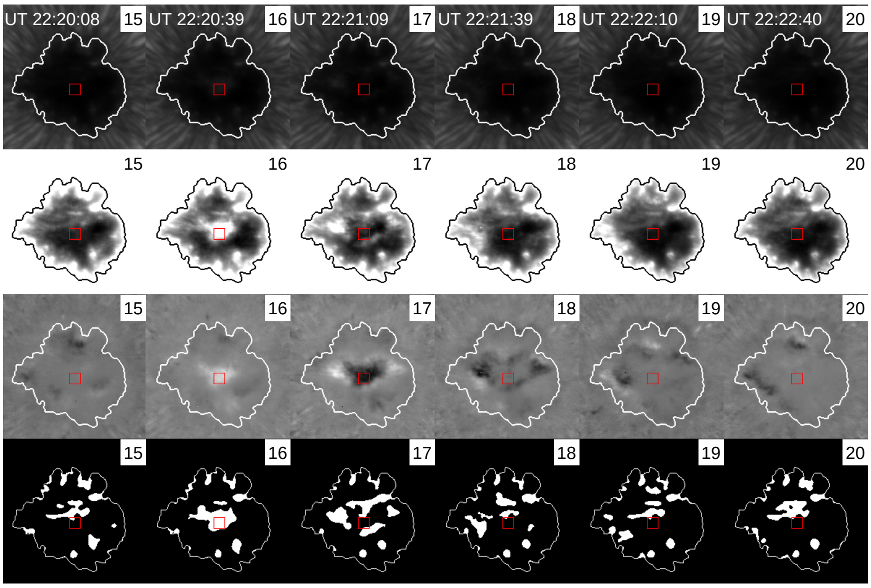

Fig. 6 An illustration of the UF that appears in the second sequence.

in each frame. The results are shown in Figure 7(a) and (b), respectively. The intensity profiles show a periodical variation. The oscillation frequencies of Umbra A and Umbra B are 2.5 min (6.6 mHz) and 3 min (5 mHz), respectively. Although both of these cases are only shown here, the variation of the case shown in Figure 6 is similar. The results entirely agree with previous reports (e.g. Socas-Navarro et al. 2009; Liang et al. 2011; Bharti et al. 2013). This further demonstrates that using our proposed method to identify and locate the emission source position of UFs is accurate and efficient, and it is easy to extract properties of UFs.

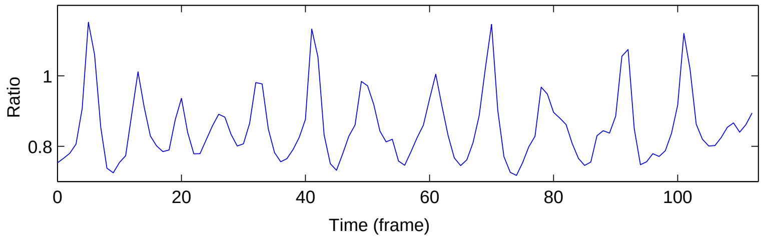

(a)

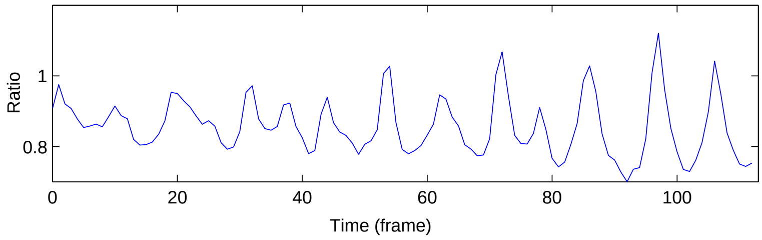

(b)

Fig. 7 Intensity variations in (a) the emission sources of UFs that is shown in Fig. 4 and (b) in Fig. 5.

5 CONCLUSIONS

Accurate identification of emission sources of UFs is crucial for investigating UFs, running penumbral and umbral waves, and their relationships, as well as the correspondence between UFs and umbral dots in the solar photosphere. Objectively defining their shapes is very troublesome because the UFs have low contrast with respect to their surroundings and also have a relatively low luminance, so it is extremely difficult to locate their positions by the classical identification methods based on intensity and gradient. Because of this, we proposed a novel method, employing the LWMPA measure based on the PC technique, to identify emission sources of UFs. For illustrating the performance, we first compared the analysis results obtained by our proposed method with traditional identification methods. Following this, our method was applied to two time sequences of Ca II H images to evaluate the performance. Finally, we calculated the intensity variation of the emission sources.

Our analysis results demonstrate that the LWMPA measure can resist changes in image contrast or luminance to identify the shape of features by phase, rather than by intensity or contrast. The measure can better describe the shape of features in different intensity levels. Therefore, we can easily identify and locate the bright patches of UFs more accurately and efficiently. Meanwhile, we can objectively define the boundary of the bright patches and extract their properties, like area and intensity, without prior knowledge about their intensity, position or morphology. Based on this, we can use them to further study the physical mechanism of the emission sources and the relations to the running umbral waves and running penumbral waves, as well as umbral dots.

Solar observations generally show dramatic variations in luminance and contrast in an image. Our proposed method can also be used to identify the shape of many other phenomena with both low contrast and low luminance, like off-limb coronal loops, umbral dots and so on.

Acknowledgements The authors are grateful to the referee for enlightening comments and suggestions that improved the quality of our work. This work is supported by the National Natural Science Foundation of China (Nos. U1231205, 11163004, 11263004 and 11303011) and the Open Research Program of Key Laboratory of Solar Activity of Chinese Academy of Sciences (No. KLSA201309). This work is also supported by the Opening Project of Key Laboratory of Astronomical Optics

& Technology, Nanjing Institute of Astronomical Optics & Technology, Chinese Academy of Sciences (No. CAS-KLAOT-KF201306). *Hinode* is a Japanese mission developed and launched by ISAS/JAXA, with NAOJ as a domestic partner and NASA and STFC (UK) as international partners. It is operated by these agencies in cooperation with ESA and NSC (Norway).

References

Beckers, J. M., & Tallant, P. E. 1969, Sol. Phys., 7, 351
Bharti, L., Hirzberger, J., & Solanki, S. K. 2013, A&A, 552, L1
Brisken, W. F., & Zirin, H. 1997, ApJ, 478, 814
Kneer, F., Mattig, W., & v. Uexkuell, M. 1981, A&A, 102, 147
Kovesi, P. 1999, VIDERE: Journal of Computer Vision Research, 1, 1
Kovesi, P. 2000, Psychological Research, 64, 136
Liang, H., Ma, L., Yang, R., Li, H., & Zhao, L. 2011, PASJ, 63, 575
Liang, H. F., Yang, W. G., Ma, L., & Yang, R. J. 2012, New Astron., 17, 112
Moore, R. L. 1973, Sol. Phys., 30, 403
Morrone, M. C., & Owens, R. A. 1987, Pattern Recognition Letters, 6, 303
Morrone, M. C., Ross, J., Burr, D. C., & Owens, R. 1986, Nature, 324, 250
Nagashima, K., Sekii, T., Kosovichev, A. G., et al. 2007, PASJ, 59, 631
Oppenheim, A. V., & Lim, J. S. 1981, Proceedings of the IEEE, 69, 529
Rouppe van der Voort, L. H. M., Rutten, R. J., Sütterlin, P., Sloover, P. J., & Krijger, J. M. 2003, A&A, 403, 277
Socas-Navarro, H., McIntosh, S. W., Centeno, R., de Wijn, A. G., & Lites, B. W. 2009, ApJ, 696, 1683
Spruit, H. C. 1981, in The Physics of Sunspots, eds. L. E. Cram, & J. H. Thomas, 98
Tsuneta, S., Ichimoto, K., Katsukawa, Y., et al. 2008, Sol. Phys., 249, 167
Tziotziou, K., Tsiropoula, G., Mein, N., & Mein, P. 2007, A&A, 463, 1153
Wittmann, A. 1969, Sol. Phys., 7, 366
Zharkov, S., Zharkova, V. V., & Ipson, S. S. 2005, Sol. Phys., 228, 377